Article

Atmospheric Mercury Pollution in the Xi'an Area, China, Studied by Differential Absorption Lidar

Zheng Duan [1,2,3], Guangyu Zhao [1,2], Shiming Zhu [1,2], Ming Lian [1,2], Yiyun Li [1,2], Weixing Zhang [4] and Sune Svanberg [1,2,5,*]

[1] National Center for International Research on Green Optoelectronics, South China Normal University, Guangzhou 510006, China; zheng.duan@coer-scnu.org (Z.D.); guangyu.zhao@coer-scnu.org (G.Z.); shiming.zhu@coer-scnu.org (S.Z.); lianming@udel.edu (M.L.); yiyunli@tamu.edu (Y.L.)

[2] Guangdong Provincial Key Laboratory of Optical Information Materials and Technology & Center for Optical and Electromagnetic Research, South China Academy of Advanced Optoelectronics, South China Normal University, Guangzhou 510006, China

[3] Innovation Academy for Microsatellites, Chinese Academy of Sciences, Shanghai 201203, China

[4] Emperor Qin Shihuang's Mausoleum Museum, Xi'an 710600, China; zwxing666@aliyun.com

[5] Department of Physics, Lund University, SE 221 00 Lund, Sweden

[*] Correspondence: sune.svanberg@fysik.lth.se

Abstract: Measurements of the atmospheric concentration of polluting atomic mercury were performed using the differential absorption lidar (DIAL) technique in the Lintong district, about 35 km northeast of Xi'an, the capital of the Shaanxi province, China. Concentrations ranging from 2 to 13 ng/m^3 were observed. As uniquely enabled by the lidar technique, representative average concentrations, integrated over a considerable volume, were recorded and put in relation to weather conditions, and vertical concentration profiles were measured. Considerable local non-uniformities were also observed, which may indicate the presence of localized hot-spots in the area, possibly related to ancient tombs.

Keywords: mercury; pollution; lidar; remote sensing; Xi'an

1. Introduction

Mercury is a serious global heavy metal pollutant with a strong impact on humans and the ecosystem. Mercury finds many areas of utilization including in instruments, as a liquid electrode in chlor-alkali plants, as a catalyst, as a tooth-filling material, and for extraction of gold from ores. In view of its many serious health effects, as flagrantly demonstrated, e.g., by the Minamata Bay catastrophe [1], Iraqi poisoning events [2], etc., the use of mercury is currently being strongly reduced, and in many countries a complete ban has been introduced [3–5]. Globally, the annual supply of mercury was about 5000 tons in 2015, with about 2000 tons coming from mining. China is the largest consumer of mercury [6]. Mining operations at many of the major production sites, including Almadén (Spain), Abbadia San Salvatore (Italy), Idrija (Slovenia), and Wanshan (China) have been discontinued, but cleaning up efforts mostly remain a heroic task. However, new mines are instead being opened up, e.g., in Mexico and Indonesia [6].

Mercury enters the environment as an atmospheric pollutant or as a water and soil pollutant, which is absorbed and integrated in plants, animals, and humans. Methyl mercury CH_3Hg^+ is a particularly toxic compound, with a strong adverse influence on the brain and nervous system [7]. Much of the mercury pollution primarily enters the atmosphere from coal-burning plants, waste incinerators, mining, metal processing plants, and electrochemical industries, etc. One final fate of the pollutant, which up to 90 percent is present as free atoms while in the atmosphere [8,9], is its conversion into the very dangerous methyl mercury.

Mercury pollution is much studied, resulting in a very extensive scientific literature. Large international conferences are arranged biannually, with the latest one in 2019 [10]. The situation in China is discussed, e.g., by Streets et al. [11], Feng [12], and Zhang and Wong [13]. Gaseous atmospheric mercury is the subject of many studies using conventional sampling techniques; see, e.g., [14–19]. Atomic mercury in the atmosphere can also be studied with high sensitivity by the remote sensing technique lidar (light detection and ranging), as pioneered by the Lund University lidar group [20], and applied in many studies, especially concerning total mercury flux assessments, e.g., at chlor-alkali plants [21] or from geothermal installations or mercury mines [22]. The differential absorption lidar (DIAL) technique, which provides spectroscopic species identification, is employed [23].

Recently, advanced DIAL technology suitable for the challenging task of atomic mercury monitoring has become available in the Chinese environment through the work of the Applied Laser Spectroscopy and Remote Sensing group at South China Normal University (SCNU) [24]. In particular, a mobile lidar system with mercury DIAL capability has been constructed [25], and urban mercury pollution measurements have been performed in Guangzhou and Zhengzhou [25–27]. Further, measurements at the strongly polluted Wanshan (Guizhou) mining area have recently been pursued [28]. The range resolution attainable with a DIAL system depends on the concentration and the absorption cross section of the gas under study, as becomes evident from the Beer–Lambert law, which governs all absorption measurements. Since the cross section for atomic mercury is very high, it becomes possible to measure atomic mercury down to the Atlantic background concentrations of 1–2 ng/m^3 [29], but then with a very crude range resolution interval, typically hundreds of meters. The range resolution intervals attainable are correspondingly smaller for higher concentrations [23].

The present paper presents extensive measurements of atmospheric atomic mercury in the area of the major Chinese city of Xi'an, and more specifically within Lintong, about 35 km, northeast of the city, as a base. The study of the Xi'an area atmospheric mercury pollution was performed in conjunction with an archaeology-motivated lidar study of possible mercury emission from the first Qin emperor mausoleum in Lintong, which has just been reported separately [30]. While that study relates to the use of mercury as a geophysical tracer gas, the present one gives first results on the concentration of atomic mercury pollution in the Xi'an atmosphere, while soil and water mercury pollution in this area has previously been studied [31]. We put our findings in relation to earlier studies of mercury in major Chinese cities. In particular, we were interested in finding possible influences from archaeological features, other than the main mausoleum, and possible effects on measured mercury concentrations due to past mercury mining activities in the Lantian area.

The paper is organized as follows. We present, following this introduction, the basic principles of differential absorption lidar, and how the techniques can be used to determine the range-resolved concentration of specific pollutant gases. The components of our mobile lidar system, as well as the details of our measurements and the results, are described in Section 3. The observations are discussed and analyzed in a final section, where also suggestions for future work are given.

2. Principles and Methods

Derived from the Beer–Lambert law, the lidar equation can be expressed as Equation (1) [23].

$$P(\lambda, R) = \frac{P_0 K \beta(R)}{R^2} exp\left\{ -2 \int_0^R \left[\alpha'(r) + N(r)\sigma \right] dr \right\} \tag{1}$$

Here, $P(\lambda, R)$ is the light intensity of the detected signal from the distance R. P_0 is the transmitted light intensity. K is a characteristic coefficient of the lidar system, related to detection efficiency, etc. $\beta(R)$ is the coefficient of backscattering, and $\alpha'(r)$ is the extinction coefficient of the atmosphere, due to particulates and broadly absorbing species, and not related to the target gas. $N(r)$ is the concentration of the target gas at the distance r. σ is

the absorption cross section of the target gas under study. As for DIAL, two different wavelengths are intermittently transmitted from the pulsed, tunable laser. One wavelength is on the characteristic absorption line of the target gas (λ_{on}), and the other one is at a close-lying position, but off (λ_{off}) the characteristic line. The parameters P_0, $\alpha'(r)$, and K for the two different wavelengths are assumed to each have the same value, which is a very good approximation for close-lying wavelengths. The ratio between the two backscattered light intensities will yield the DIAL curve according to Equation (2):

$$P(\lambda_{on}, R)/P\left(\lambda_{off}, R\right) = exp\left\{-2\left(\sigma_{on} - \sigma_{off}\right)\int_0^R N(r)dr\right\} \tag{2}$$

Here, $P(\lambda_{on}, R)$ and $P\left(\lambda_{off}, R\right)$ represent the powers of the collected signals for the on- and off-wavelengths, respectively. σ_{on} and σ_{off} are the absorption cross sections of the target gas at the wavelengths λ_{on} and λ_{off}, respectively. The target gas concentration can be directly derived, using the known differential absorption cross section, $\Delta\sigma = (\sigma_{on} - \sigma_{off})$. The target gas concentration as a function of range can then be expressed by Equation (3).

$$N(R) = \frac{1}{-2\left(\sigma_{on} - \sigma_{off}\right)}\left\{\frac{d}{dR}\left\{ln[\frac{P(\lambda_{on}, R)}{P\left(\lambda_{off}, R\right)}]\right\}\right\} \tag{3}$$

After averaging and filtering, the ratio is locally fitted by an exponential function over a chosen resolution interval, and the concentration can be calculated. Expressed simply, the concentration of the target gas is closely related to the slope of the ratio curve. Clearly, the accuracy in the concentration evaluation is then dependent on the range integration interval chosen and the signal-to-noise level in the recorded curves, which is range-dependent because of the $1/R^2$ signal fall-off.

3. Measurements and Results

3.1. Measurement System

Our atomic mercury measurements were performed with the new SCNU mobile differential absorption lidar system. Since the system and its performance are described in detail in [25], only a brief description will be given here. The system, which is installed in a laboratory container module, carried by a Jiefang truck, is equipped with a Nd:YAG laser, which operates with a repetition frequency of 20 Hz. The fundamental wavelength is 1064 nm, and harmonics at 532, 355 and 266 nm can be generated with the use of nonlinear crystals. The third harmonic output at 355 nm was used to pump a tunable dye laser operating with the dye Coumarin 307 for the generation of light at 508 nm. Finally, after frequency doubling, we obtained laser radiation close to 254 nm, matching the strong atomic mercury transition $6s^2\,{}^1S_0 - 6s6p\,{}^3P_1$ while avoiding interference from close-lying atmospheric molecular oxygen lines. Spectroscopic considerations, and absorption cross section aspects, have been discussed by [24]. In order to collect the backscattered light from atmospheric particulates and major molecular species, a vertically looking 400 mm-diameter Newtonian telescope is used in combination with a roof-top folding mirror, which is controlled by stepping motors, allowing 360° horizontal scanning and vertical scanning from −10° to 45°. Temperature, wind direction, and speed were recorded continuously during most of the measurements, using a Misol model WA1091 weather station. The SCNU lidar system is believed to be the only one presently available worldwide for range-resolved atmospheric mercury monitoring.

A good agreement between mercury DIAL data from our new mobile system and the recordings of a commonly used point monitor, which is based on Zeeman modulation techniques applied to the 254 nm mercury resonance line, has earlier been demonstrated [28].

3.2. Measurement Site

The measurement site and the positioning of the lidar system are shown in Figure 1, where the site location with regard to the city of Xi'an and a neighboring mercury mine is indicated (Figure 1a). The closer neighborhood at the measurement site is shown in Figure 1b, where three different locations of the system during measurements are indicated. The green dashed line actually outlines the pyramid-shaped mausoleum of Emperor Qin, who unified China and ruled from 221 to 210 B.C. This site became of particular interest after the 1974 discovery of the 8000 men strong terracotta army, protecting the tomb. According to historian Sima Qian [32], who 2200 years ago wrote the historical account on Emperor Qin, large amounts of liquid mercury had been introduced into the tomb chamber before closure. The hypothesis that this mercury might have left an imprint by migration also to the mausoleum surface, motivated a very recently published study by [30], where, indeed, elevated atomic mercury levels were found at the upper parts of the mound. That study relates to archaeology only, while the present investigation addresses the mercury pollution situation in the atmosphere of the major Chinese city of Xi´an.
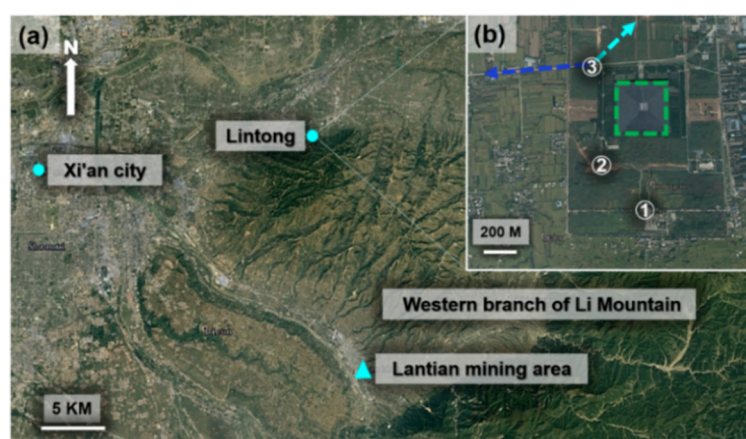

Figure 1. Overview schematic of the measurement site in the Lintong district of Xi'an city. (**a**) The location with respect to Xi´an city and a mercury mine location. (**b**) Close-up of the Lintong district. The three spots labelled with different numbers indicate the different locations of the lidar system during measurements, while the green, dashed line marks the position of the emperor Qin mausoleum mound. A 360° scanning monitoring was conducted at site 1. Vertically resolved measurements of the concentration were made at site 2. Finally, from site 3, the atmospheric mercury content in two different directions was measured, with one pointing towards the urban area and the other one towards the suburban area.

3.3. Sample Differential Absorption Lidar Recording

Extensive range-resolved monitoring of atmospheric mercury was performed by intermittently transmitting laser radiation at the strongly absorbed wavelength and at the nearby non-absorbed reference wavelength. The on-wavelength was set to 253.728 nm and the off-wavelength to 253.745 nm in our measurements, and the differential optical absorption cross section adopted for the data evaluation was 2.5×10^{-14} cm^2 atom^{-1} [24].

An example of raw data is shown in Figure 2, where the DIAL curve, which was obtained by divided the lidar return signal for the absorbed wavelength by the one obtained for the non-absorbed one, is also plotted. Further, evaluated range-resolved concentration values are calculated from the slope of the DIAL curves as expressed by Equation (3) [23], and shown in green in the figure. Data evaluation was initiated at a range of 100 m, since for closer ranges small laser beam spatial overlap deviations as well as possible saturation of the atomic transition degrade the data accuracy. The concentration evaluation was performed on the smoothed DIAL curve with an effective range interval of 75 m [30]. As noted in connection with Equation (3), the accuracy in the concentration evaluation

from DIAL data depends on many factors, and is typically ± 1–2 ng/m^3 depending on evaluation range for conditions pertaining to the data given in Figure 2.
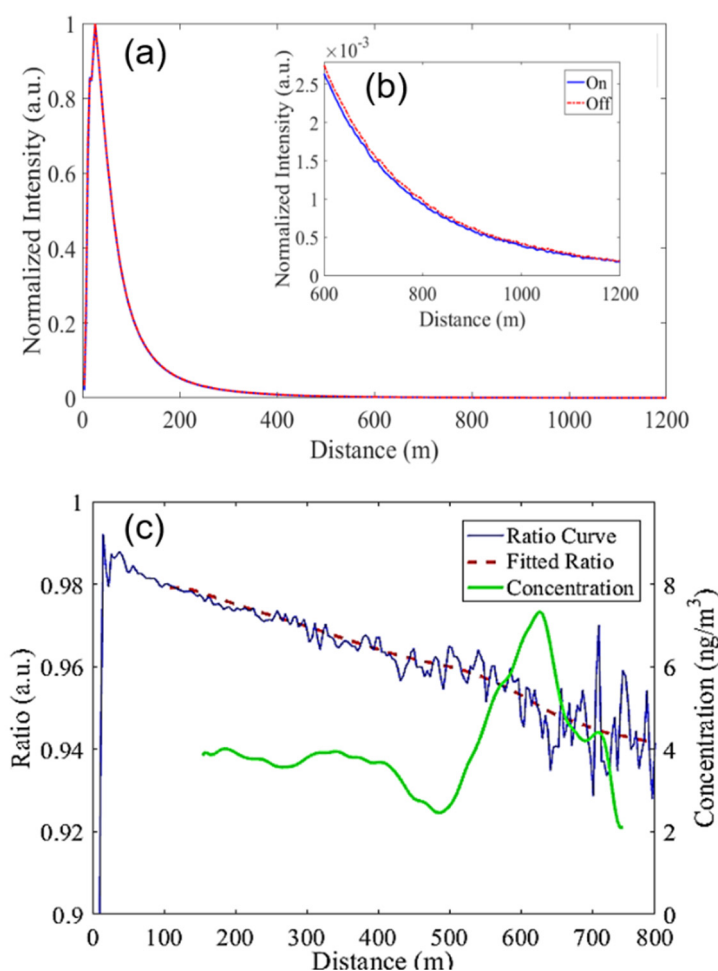

Figure 2. Example of measurement data; (**a**) lidar returns for the on- and off-resonance wavelengths are shown; (**b**) zoom-in of on- and off-resonance curves from 600 to 1200 m; (**c**) DIAL curve, obtained by dividing the on- by the off-resonance lidar returns; fitted ratio and concentration calculated from the DIAL curve. The total data integration time was 5 min, corresponding to 6000 averaged transients and resulting in the range-resolved concentration curve, where the sliding integration interval was about 75 m.

3.4. Area Surveillance Measurements

The 360° scanning monitoring of the surrounding atomic mercury was performed at measurement site 1 in Figure 1b, using the 40 cm diameter Newtonian telescope with the folding mirror controlled by the stepping motors. The reference direction was chosen as the highest structure around the lidar system, the peak of the western branch of the Li Mountain in the south, and scanning ran clockwise. By adjusting the folding mirror, the elevation angle was fixed at about 5° from the horizontal direction. The measuring distance covered 100 to 600 m, and in the concentration evaluation, a sliding integration interval of 75 m was used. The wind direction was north–east and east with speeds varying between 0.3 and 3.3 m/s, and the local temperature was about 29 °C. The 360° scanning area was evenly separated in 60 steps each of 6°, and the sampling time period was 7 min. The results are presented in Figure 3, with concentrations reaching up to 13 ng/m^3. Hotspots of relatively high mercury concentrations might be due to the excavation pits in the Qin mausoleum park. This assumption may be supported by an earlier study, where soil gas was extracted

from 70 cm deep holes drilled into the ground in the Qin mausoleum area revealing sites with concentrations of mercury in the gas in the 100 ng/m^3 range [33,34].
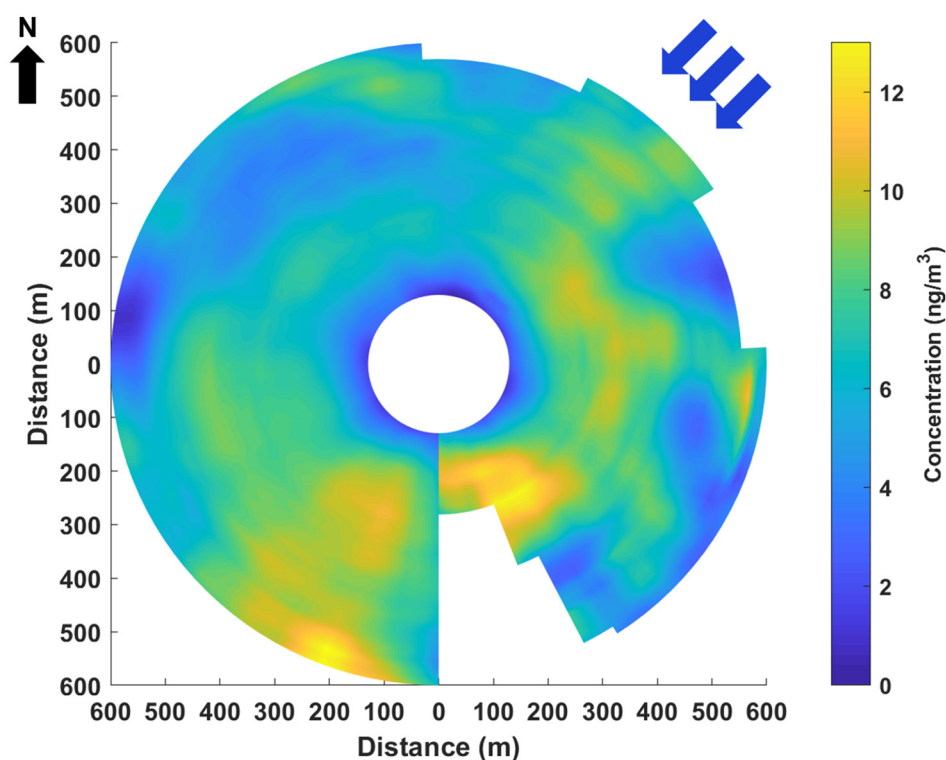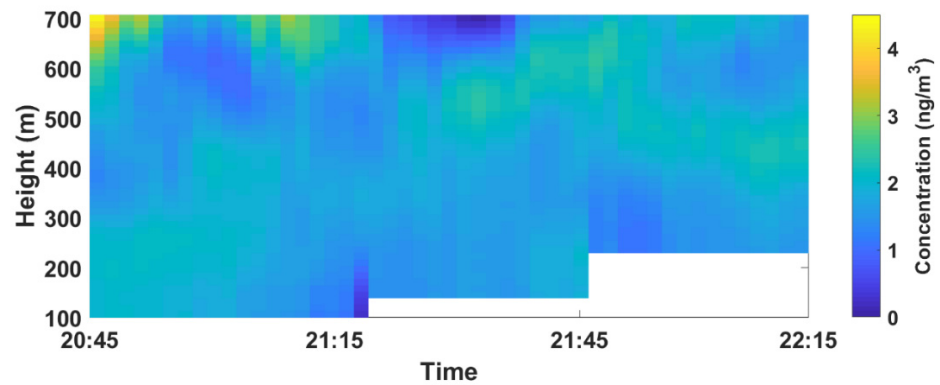

Figure 3. The 360° mapping of mercury concentration from 21:30 August 4, to 6:30, August 5, 2016. Each sector is averaged for 7 min with 60 sectors altogether. The wind direction was from the northeast as indicated in blue arrows. In certain directions, the range covered is more limited; this is particularly true in the south–east direction, where the strongly increased light background level due to the early morning sun impaired the available signal-to-noise ratio. The concentrations were measured along the laser beam, which had an elevation of about 5 degrees corresponding to 10–55 m height for the 100–600 m range. The concentration value range resolution was 75 m.

3.5. Vertical Monitoring

Vertical monitoring was conducted at monitoring site 2 by removing the top folding mirror and letting laser pulses be transmitted into the sky vertically. The monitoring was performed from 20:45 to 22:15, 13 August, 2016. The vertical monitoring was made in three time segments, and for each one, the duration was about 30 min. The second and third measurements were made with electronic delays introduced. The reason for the delay setting was an attempt to measure to further height by increasing the voltage of the photomultiplier detector, which then causes the close-range signal to go off-scale. However, the attempt was not successful, since the far-range signal-to-noise level for the available laser pulse energy was insufficient.

The wind direction was south–east, and the local temperature was about 38 °C. The results are shown in Figure 4. The vertical concentration distributions of mercury, ranging from 100 to 700 m in height, were up to about 5 ng/m^3. The variation in the mercury concentration and the absence of a clear vertical gradient might be due to the strong air convection during the very hot day. We noted that the wind trajectories from the 25 km distant Lantian mercury mine (indicated in Figure 1) would pass close to the measurement site, but somewhat to the west. We did not observe any significant influence from the mine. This is in strong contrast to the observations in an earlier study, where, however, the locations of mines and a smelter plant were much closer [28].

Figure 4. Vertical monitoring of mercury concentrations at the second measurement site 2. Clear and varying concentration structures could be observed, while aerosols exhibited little structure. The wind direction was from south to east.

3.6. Urban–Suburban Comparison

Mercury monitoring in two different directions at the third measurement site was performed on 18 August 2016. The local temperature was about 38 °C, and the wind was from north to east at a speed of 3 m/s. As shown in Figure 5, one measurement direction (used from 10:30 to 11:00 a.m.) was towards the suburban area, and the other one (used from 11:10 to 11:40 a.m.) was towards the urban area of the Lintong district. The reachable measurement distance was about 600 m. We found from the recordings that the mercury concentration in the suburban direction stayed more uniform at around 4 ng/m^3; while in the urban direction, the mercury concentration became higher, up to 8 ng/m^3, as the location got closer to the urban area. While this observation is not unexpected, given the stable wind conditions during the measurements, concentrations can be influenced by several factors including localized sources not related to urban conditions specifically.
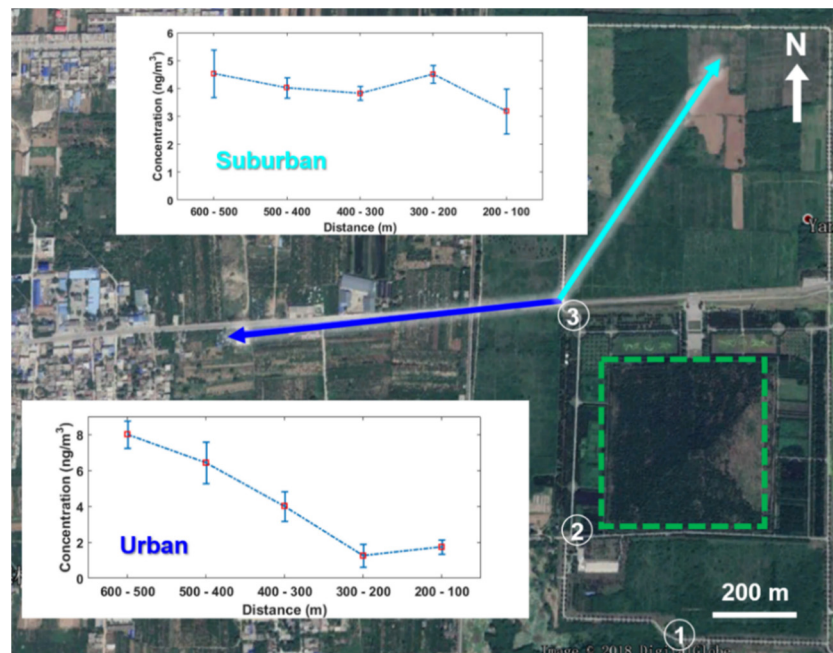
Figure 5. Comparison of mercury concentrations in two different directions. The light blue arrow is directed towards the suburban area and the blue arrow towards the Lintong urban area. The green dashed line indicates the position of the emperor Qin tomb mound.

3.7. Representative Monitoring over a Time Period of Two Weeks

Mercury concentration monitoring measurements were performed in the Qin mausoleum park during the night hours (21:00–1:00) from 27 July to 12 August, and the average concentration results are shown in Figure 6. The mean concentration from all the measurements during the four selected hours every day was plotted with one standard deviation error bars. The beam elevation was about 5 degrees, and the concentrations were averaged for the 100–600 m range along the beam, which was scanning over the mound. The average corresponding temperature and wind speeds are also shown. At the first measurement site, mercury monitoring was conducted from 27 July to 4 August. Then, we moved to the second measurement site and continued to monitor the mercury concentration over the area from 7 August to 12 August. During the measurements of the mercury concentration, the weather changed from time to time. The measurements were stopped when it was raining hard, because of very strong scattering from raindrops and associated reduction in the measurement range; we continued to monitor when it stopped raining. The concentration of mercury decreased somewhat after rain, an observation, which is consistent with earlier findings [26]. The average precipitations in the three rainy periods, as presented in Figure 6a and based on the recorded weather data, are 4.7, 4.1, and 1.9 mm per day. The average mercury concentrations during the four selected hours of the three days following the rain are 3.54 ± 0.96 ng/m^3, 4.55 ± 0.77 ng/m^3, and 3.92 ± 0.57 ng/m^3. The local average atmospheric mercury concentration remained relatively stable, and mostly in the range from about 3 to 7 ng/m^3 during the hot weather conditions during our campaign. The wind conditions did not obviously affect the mercury concentrations. The representative time series presented with interruptions by precipitation is the longest one recorded by mercury lidar to date.
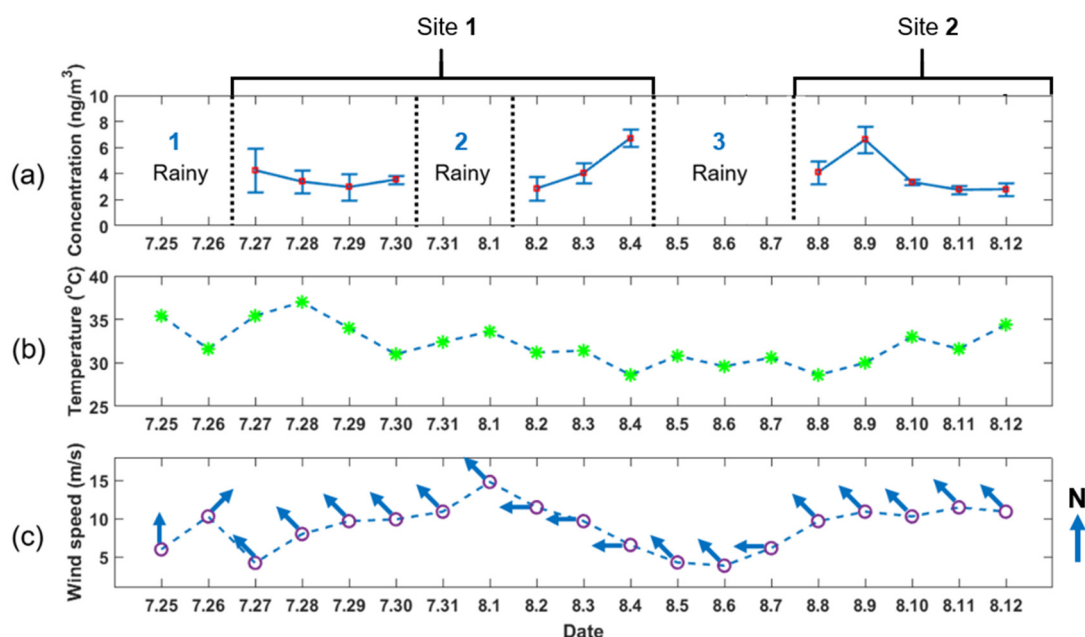
Figure 6. (**a**) Mercury average concentration in the Qin mausoleum area during a period with weather changes; (**b**) temperature change and (**c**) wind speed variance during the monitoring period; the blue arrows in (**c**) indicate the wind direction. Weather data are from the local Lintong weather service.

4. Discussion and Conclusions

The SCNU mobile differential absorption lidar (DIAL) system was successfully used in this campaign to map a large-area atmospheric mercury pollution distribution, to study concentration variations with time and under different climatic conditions, and assess the vertical concentration. Ambient mercury concentrations in the Lintong area (Xi'an)

varied in the 2 to 13 ng/m^3 range and were on average comparable to those recorded in other major Chinese cities (see, e.g., [24–27,35]). Remarkably strong spatial variations of atmospheric mercury in the area surrounding the Qin mausoleum were noted (Figure 3), which might be related to localized mercury hot spots of archaeological origin in the mausoleum park, apart from those observed by us in a dedicated study of the Qin mausoleum mound [30]. The highest concentrations related to the mound itself were measured to 27 ng/m^3, which is significantly higher than observed anywhere in the present study of the mound surroundings. Still, these indications of additional hotspots, towards the east, and especially towards the south, with concentrations reaching 10 and 13 ng/m^3, respectively, warrant a closer archaeological atmospheric mercury survey of the surrounding areas, and such activities are now in planning. Using the information now obtained, a hand-held atomic mercury monitoring device, based on Zeeman modulation techniques, as employed, e.g., in our studies at Wanshan [28], could be used for real-time mapping with very high spatial resolution. Such studies might reveal the real origin of localized elevated concentrations.

We did not observe any significant influence of earlier mercury mining activities in Lantian, about 25 km from the measurement site. As noted above, while the wind trajectory for the prevailing wind during the recording of the data in Figure 3 would pass somewhat to the west of the measurement site, turbulence and fluctuations in the wind direction would have made an outflow of mercury of the same magnitude as observed in Wanshan noticeable. As a matter of fact, no wind-dependent influence from the mining area was observed throughout the study period. Clearly, a detailed lidar study on the Lantian site would also be of considerable interest.

Our measurements are, to our knowledge, the first ones on free atomic mercury in the open atmosphere in this area, and clearly the first ones performed by differential absorption lidar techniques. However, gas extracted from 70 cm deep drilled holes into the ground has earlier been studied in the area of the Qin mausoleum [33,34]. The mercury was then concentrated by amalgamation on gold, and was subsequently spectroscopically measured when released on heating. Traverses covering the tomb mound revealed hotspots up to around 100 ng/m^3, but also in areas around it locations with up to around 50 ng/m^3 were identified. These earlier observations, together with the findings by Liu et al. [36] at a different archaeological site, provide further impetus for the study of atomic mercury gas related to archaeology.

Some effects of rain were observed, as also earlier observed, and then even more prominently [26]. Since atomic mercury is not very soluble in water, the reduction may rather be related to indirect effects of soil cooling and atmospheric changes. The wind speed and direction did not strongly affect the average mercury concentrations, as given in Figure 6, which would be expected, if the conditions at the measurement site were similar to those pertaining to the area around. This also indicates that although hotspots were identified, the archaeological structures in the Qin mausoleum area do not seem to contribute significantly to the average atmospheric mercury contents in the area, which we actually found to be similar to those in other major Chinese cities—Hangzhou, Guangzhou, and Zhengzhou [24–27,35]. The conclusion regarding the possible additional atmospheric influence of the famous Xi´an archaeological site would thus be similar to what is earlier stated regarding its influence on water and soil [31].

The localized mercury–gas hotspots with concentrations exceeding 20 ng/m^3, as found in our studies at the Qin mausoleum [30], illustrate the capability of differential absorption lidar to quickly reveal underground structures of interest remotely, and considerably more conveniently than by extracting gas from numerous drilled holes into the ground. The potential application of discovering valuable ore deposits or geothermal energy by surface mercury monitoring is a further intriguing aspect of the use of atomic mercury as a geophysical tracer gas, now based on the co-location of such phenomena with volatile mercury [22,37]. Further improvements of the mechanical scanning of our system could allow faster concentration profiling and easier operation, which would further increase

the capability of our system. Most data presented in this paper were recorded during night-time, when the ambient light level was low. This was advantageous, since the 254 nm interference filter used in front of the detector unfortunately did not adequately suppress visible radiation. With a better suppression of such light, day-time operation would be equally convenient, since the ambient light at 254 nm is zero due to the absorption of the earth´s ozone layer.

The SCNU system is believed to be the only one world-wide, presently available for the demanding task of range-resolved atmospheric atomic mercury mapping. Such a system can be an asset in the quest to control the wide-spread pollution by the particularly serious neuro-toxic agent mercury, but in addition could also serve in geophysical studies—both aspects being discussed in the present paper.

Monitoring of atmospheric atomic mercury is normally performed by in-situ instruments, which are based on atomic absorption or emission using the 254 nm mercury line. The sensitivity needed for measurements of the few ng/m^3 concentrations typical of ambient conditions can normally be reached only by pre-concentration of mercury on gold by amalgamation (used, e.g., in common GARDIS and TEKRAN instruments; see, e.g., [16]). However, by using extremely sensitive Zeeman modulation techniques, allowing a perfect correlation to the atomic absorption line, real-time monitoring can be achieved with LUMEX instruments (see, e.g., [28]). Such instruments allow long-term monitoring at a single location. In contrast, mercury lidar techniques allow remote-sensing, range-resolved measurements over considerable distances, and also vertical monitoring, but are clearly considerably more complex, and not suited for long-term measurements. The measurements described in the present paper illustrate some unique possibilities available with a mercury lidar system.

Author Contributions: Conceptualization, S.S. and G.Z.; methodology, S.S. and G.Z.; software, G.Z. and Z.D.; validation, G.Z., Z.D. and S.S.; formal analysis, Z.D.; investigation, Z.D., G.Z., S.Z., M.L., Y.L., W.Z. and S.S.; resources, S.S., G.Z. and W.Z.; data curation, Z.D. and G.Z.; writing—original draft preparation, Z.D. and S.S.; writing—review and editing, S.S.; visualization, Z.D.; supervision, S.S. and G.Z.; project administration, G.Z., W.Z. and S.S.; funding acquisition, S.S. and G.Z. All authors have read and agreed to the published version of the manuscript.

Institutional Review Board Statement: Not applicable.

Informed Consent Statement: Not applicable.

Data Availability Statement: The data presented in this study are available on request from the first, and the corresponding author.

Conflicts of Interest: The authors declare no conflict of interest related to this paper.

References

1. Harada, M. Minamata Disease: Methylmercury Poisoning in Japan Caused by Environmental Pollution. *Crit. Rev. Toxicol.* **1995**, *25*, 1–24. [CrossRef]
2. Marsh, D.O.; Clarkson, T.W.; Cox, C.; Myers, G.J.; Amin-Zaki, L.; Al-Tikriti, S. Fetal Methylmercury Poisoning. *Arch. Neurol.* **1987**, *44*, 1017–1022. [CrossRef]
3. Beckers, F.; Rinklebe, J. Cycling of mercury in the environment: Sources, fate, and human health implications: A review. *Crit. Rev. Environ. Sci. Technol.* **2017**, *47*, 693–794. [CrossRef]
4. United Nations. Minamata Convention on Mercury. 2013. Available online: http://www.mercuryconvention.org/Portals/11/documents/Booklets/Minamata%20Convention%20on%20Mercury_booklet_English.pdf (accessed on 26 December 2020).

5. Mazzolai, B.; Mattioli, V.; Raffa, V.; Tripoli, G.; Dario, P.; Ferrara, R.; Lanzilotta, E.; Munthe, J.; Wängberg, I.; Barregård, L.; et al. A multidisciplinary approach to study the impact of mercury pollution on human health and environment: The EMECAP project. *RMZ Mater. Geoenviron.* **2004**, *51*, 682–685.

6. UNEP. Global Mercury: Supply, Trade and Demand. 2017. Available online: http://wedocs.unep.org/bitstream/handle/20.500.1 1822/21725/global_mercury.pdf?sequence=1&isAllowed=y (accessed on 26 December 2020).

7. Committee on Toxicological Effects of Methylmercury, National Research Council of the United States, National Academies of Science. In *Toxicological Effects of Methylmercury*; National Academies Press: Washington, DC, USA, 2000.

8. Pacyna, E.G.; Pacyna, J.M.; Sundseth, K.; Munthe, J.; Kindbom, K.; Wilson, S.; Steenhuisen, F.; Maxson, P. Global emission of mercury to the atmosphere from anthropogenic sources in 2005 and projections to 2020. *Atmos. Environ.* **2010**, *44*, 2487–2499. [CrossRef]

9. Streets, D.G.; Horowitz, H.M.; Jacob, D.J.; Lu, Z.; Levin, L.; Ter Schure, A.F.H.; Sunderland, E.M. Total Mercury Released to the Environment by Human Activities. *Environ. Sci. Technol.* **2017**, *51*, 5969–5977. [CrossRef]

10. ICMGP. In Proceedings of the International Conference on Mercury as a Global Pollutant, Krakow, Poland, 8–13 September 2019.

11. Streets, D.G.; Hao, J.; Wu, Y.; Jiang, J.; Chan, M.; Tian, H.; Feng, X. Anthropogenic mercury emissions in China. *Atmos. Environ.* **2005**, *39*, 7789–7806. [CrossRef]

12. Feng, X.B. Mercury pollution in China—An overview. In *Dynamics of Mercury Pollution on Regional and Global Scales*; Pirrone, N., Mahaffey, K.R., Eds.; Springer: Norwell, MA, USA, 2005; pp. 657–678.

13. Zhang, L.; Wong, M.H. Environmental mercury contamination in China: Sources and impacts. *Environ. Int.* **2007**, *33*, 108–121. [CrossRef]

14. Wängberg, I.; Munthe, J.; Pirrone, N.; Iverfeldt, Å.; Bahlman, E.; Costa, P.; Ebinghaus, R.; Feng, X.; Ferrara, R.; Gårdfeldt, K.; et al. Atmospheric mercury distribution in Northern Europe and in the Mediterranean region. *Atmos. Environ.* **2001**, *35*, 3019–3025. [CrossRef]

15. He, K.; Huo, H.; Zhang, Q. Urban Air Pollution in China: Current Status, Characteristics, and Progress. *Annu. Rev. Energy Environ.* **2002**, *27*, 397–431. [CrossRef]

16. Feng, X.; Tang, S.; Shang, L.H.; Yan, H.; Sommar, J.; Lindqvist, O. Total gaseous mercury in the atmosphere of Guiyang, PR China. *Sci. Total. Environ.* **2003**, *304*, 61–72. [CrossRef]

17. Fu, X.; Feng, X.; Wang, S.; Rothenberg, S.; Shang, L.H.; Li, Z.; Qiu, G. Temporal and spatial distributions of total gaseous mercury concentrations in ambient air in a mountainous area in southwestern China: Implications for industrial and domestic mercury emissions in remote areas in China. *Sci. Total. Environ.* **2009**, *407*, 2306–2314. [CrossRef]

18. Liu, N.; Qiu, G.; Landis, M.S.; Feng, X.; Fu, X.; Shang, L.H. Atmospheric mercury species measured in Guiyang, Guizhou province, southwest China. *Atmos. Res.* **2011**, *100*, 93–102. [CrossRef]

19. Fu, X.; Feng, X.; Sommar, J.; Wang, S. A review of studies on atmospheric mercury in China. *Sci. Total. Environ.* **2012**, *421*, 73–81. [CrossRef]

20. Aldén, M.; Edner, H.; Svanberg, S. Remote measurement of atmospheric mercury using differential absorption lidar. *Opt. Lett.* **1982**, *7*, 221–223. [CrossRef]

21. Grönlund, R.; Sjöholm, M.; Weibring, P.; Edner, H.; Svanberg, S. Elemental mercury emissions from chlor-alkali plants measured by lidar techniques. *Atmos. Environ.* **2005**, *39*, 7474–7480. [CrossRef]

22. Svanberg, S. Geophysical gas monitoring using optical techniques: Volcanoes, geothermal fields and mines. *Opt. Lasers Eng.* **2002**, *37*, 245–266. [CrossRef]

23. Svanberg, S. Differential absorption lidar (DIAL). In *Air Monitoring by Spectroscopic Techniques*; Sigrist, M., Ed.; Wiley: New York, NY, USA, 1994; pp. 85–161.

24. Mei, L.; Zhao, G.; Svanberg, S. Differential absorption lidar system employed for background atomic mercury vertical profiling in South China. *Opt. Lasers Eng.* **2014**, *55*, 128–135. [CrossRef]

25. Zhao, G.; Lian, M.; Li, Y.; Duan, Z.; Zhu, S.; Mei, L.; Svanberg, S. Mobile lidar system for environmental monitoring. *Appl. Opt.* **2017**, *56*, 1506–1516. [CrossRef]

26. Zhao, G.Y.; Wu, X.X.; Lian, M.; Svanberg, S. Lidar monitoring of atmospheric atomic mercury and sulfur dioxide in Guangzhou, China. In Proceedings of the Progress in Electromagnetics Research Symposium, Guangzhou, China, 25–28 August 2014; Curran Assoc. Inc.: Red Hook, NY, USA, 2014; Volume 1–3, pp. 2711–2714, ISBN 978-1-5108-1560-5.

27. Lian, M.; Zhao, G.Y.; Li, Y.Y.; Duan, Z.; Svanberg, S.; Hu, J.D. Mobile differential absorption lidar system and the measurement of atmospheric mercury in Zhengzhou. *J. Optoelectron. Laser* **2020**, in press.

28. Lian, M.; Shang, L.H.; Duan, Z.; Li, Y.; Zhao, G.; Zhu, S.; Qiu, G.; Meng, B.; Sommar, J.; Feng, X.; et al. Lidar mapping of atmospheric atomic mercury in the Wanshan area, China. *Environ. Pollut.* **2018**, *240*, 353–358. [CrossRef]

29. Horowitz, H.M.; Jacob, D.J.; Zhang, Y.; Dibble, T.S.; Slemr, F.; Amos, H.M.; Schmidt, J.A.; Corbitt, E.S.; Marais, E.A.; Sunderland, E.M. A new mechanism for atmospheric mercury redox chemistry: Implications for the global mercury budget. *Atmos. Chem. Phys. Discuss.* **2017**, *17*, 6353–6371. [CrossRef]

30. Zhao, G.; Zhang, W.; Duan, Z.; Lian, M.; Hou, N.; Li, Y.; Zhu, S.; Svanberg, S. Mercury as a Geophysical Tracer Gas-Emissions from the Emperor Qin Tomb in Xi'an Studied by Laser Radar. *Sci. Rep.* **2020**, *10*, 10414. [CrossRef]

31. Jin, Y.; Wang, X.; Lu, J.; Zhang, C.-X.; Duan, Q. Effects of modern and ancient human activities on mercury in the environment in Xi'an area, Shannxi Province, P.R. China. *Environ. Pollut.* **2008**, *153*, 342–350. [CrossRef]

32. Qian, S. Translated by William Nienhauser Jr. et al. as The Grand Scribe's Records. In *The Basic Annals of Pre-Han China*; Indiana University Press: Bloomington, IN, USA, 1994; Volume 1, p. 127, ISBN 0253340217.

33. Liu, C.M.; Shi, C.Y.; Hu, S.Q.; Yan, W.D. Mercurometric survey and α-cup radon measurement in archeological detection of the Qin Shi Huang tomb. *Geophys. Explor.* **2005**, *29*, 336–341.

34. Xie, X.J.; Chang, Y.; Cheng, Z.Z. Mercury in Qin mausoleum: Whether there existed mercury and whence the mercury. *Geol. Bull. China* **2013**, *32*, 1485–1492.

35. Guan, Z.; Lundin, P.; Mei, L.; Somesfalean, G.; Svanberg, S. Vertical lidar sounding of atomic mercury and nitric oxide in a major Chinese city. *Appl. Phys. A* **2010**, *101*, 465–470. [CrossRef]

36. Liu, H.Z.; Yang, F.; Zhang, X.J.; Kong, M.; Yu, J.S.; Zhang, H. The application of mercury vapor survey to archeological detection of the Spring-Autumn tomb in Hancheng City. *Geophys. Geochem. Explor.* **2013**, *37*, 670–674. (In Chinese)

37. McCarthy, J.H. Mercury vapor and other volatile components in the air as guides to ore deposits. *J. Geophys. Explor.* **1972**, *1*, 143–162. [CrossRef]